Electronic Research Archive

https://www.aimspress.com/journal/era

ERA, 32(9): 5157–5175.
DOI: 10.3934/era.2024238
Received: 14 July 2024
Revised: 19 August 2024
Accepted: 27 August 2024
Published: 02 September 2024

Research article

Frequency analysis of a discrete-time fast nonlinear tracking differentiator algorithm based on isochronic region method

Zhizhou Zhang[1,*], Yueliang Pan[1], Weilong Zhao[1], Jinchu Zhang[1], Zheng Zi[1], Yuan Xie[1] and Hehong Zhang[2]

[1] School of Aeronautics and Astronautics, Sun Yat-sen University, Shenzhen 518107, China

[2] College of Computer and Data Science, Fuzhou University, Fuzhou 350108, China

* **Correspondence:** Email: zhangzhzh25@mail.sysu.edu.cn.

Abstract: In fault detection, feedback control, and other fields, real-time differential estimation of a given signal in a complex noise environment is an important but challenging task. In this paper, a discrete-time fast nonlinear tracking differentiator (FNTD) based on hyperbolic tangent functions was proposed. To start, the differential signal acquisition problem was equated to the time-optimal control (TOC) law for constructing a double-integral system using a state feedback approach. Next, the FNTD algorithm based on the hyperbolic tangent function was presented by utilizing the isochronic region (IR) method in the discrete time domain. Then, the frequency-domain characteristics of the FNTD were analyzed and the rule for tuning the parameters was provided by the frequency scan test method. Finally, the simulation results demonstrated that the proposed FNTD had fast and accurate tracking performance, as well as excellent filtering and differential extraction capability compared with other differentiators.

Keywords: fast nonlinear tracking differentiator (FNTD); isochronic region (IR) method; control synthesis function (CSF); frequency-domain characteristics; frequency scan test

1. Introduction

Real-time differentiation estimation of measured signals is critical and challenging in signal processing, fault diagnosis, fault control, and many other fields [1–4]. In practice, engineers often use the numerical difference method to directly approximate the differential of a measurement signal. When the sampling period T is reduced, the approximation accuracy of the differential signal tends to increase. However, differential operations inherently capture the rate of change of a signal, thus in the presence of noise, minor fluctuations in the noise can be greatly magnified through these operations. This magnification can lead to distortions in the differential results, potentially compromising the ac-

curacy and reliability of the overall system [5]. Specifically when it comes to proportional-integral-derivative (PID) control, a method that has been extensively employed since the previous century, engineers frequently resort to directly utilizing the numerical difference method to acquire differential information. However, this approach is highly susceptible to signal noise, often leading to distortions in the differential results [6]. In the absence of a superior differentiator, PID control frequently degenerates into PI control in numerous instances, resulting in a significant decline in the feedback control effect. This underscores the need for fast and accurate differentiation techniques to ensure optimal performance in PID control systems [7].

To deal with this, researchers have proposed many different approaches for differentiator design such as the high-gain observer via differentiator [8, 9], the robust exact differentiation based sliding mode [10, 11], the robust differentiator based extended Kalman filter [12], adaptive tracking differentiator [13, 14], and so on [15–17]. Among them, the linear high-gain differentiator, designed by Kahlil, provides derivatives of signals from 1 to n-1, but each derivative may contain disturbances, leading to poor anti-interference ability [18]. Linear tracking differentiator (TD) converges faster when the system state is far from the equilibrium point, but slower as it approaches [19]. Levant introduced a second-order sliding mode TD, which exhibits strong robustness and high precision. However, the rapid switching of system variables with small amplitudes near the sliding mode surface can easily lead to chattering [20]. Wang and Zhang developed a hybrid TD, integrating linear and nonlinear elements, which exhibits rapid convergence and superior noise suppression, making it suitable for aircraft speed detection [21, 22].

Furthermore, Han initially proposed a nonlinear TD that utilizes the method of time optimal control (TOC), commonly referred to as $fhan$-TD [1,23]. The TOC law of $fhan$-TD is not strictly a bang-bang control as it incorporates a linear region to facilitate a smoother transition to the extreme value [24]. Equipped with this unique characteristic, $fhan$-TD not only efficiently tracks the output signal with minimal delay but also effectively retrieves the differentiation from signals contaminated by noise and discontinuities. In practical applications, $fhan$-TD, along with an extended state observer and transient profile generator, forms an automatic disturbance rejection controller (ADRC). This controller has been successfully employed in various scenarios, including speed control of permanent-magnet synchronous motors [25,26] and induction motor drives [9,27], vehicle suspension displacement detection [28], and improved Tornambe controller for pneumatic muscle actuators [29].

In the TD algorithms, the control synthesis function (CSF) plays a crucial role in achieving fast speed, low delay, and high accuracy. Han [1, 23] derived the general form of the control synthesis function of $fhan$-TD by the state feedback method. Xie et al. [30, 31] constructed a simple linear function, referred to as $fast$-TD, by examining the boundary characteristic points of the linear area, where the control law takes non-extreme values. It should be noted that the $fast$-TD algorithm avoids the complex root operation. Zhang et al. [32] chose the appropriate control quantity based on the initial point position, determined the corresponding boundary and characteristic curves, and further derived a linearization criterion to introduce a TD featuring a straightforward structure.

An improved CSF can enable the differentiator to achieve better signal tracking and differential extraction results. From the perspective of the CSF, this paper introduces a novel fast nonlinear tracking differentiator (FNTD) with the hyperbolic tangent function. This TD employs a state feedback approach to determine the boundary curve of the linear region, the control characteristic curve, and the control laws governing both the reachable area and the linear area.

This paper is organized as follows: Section 2 introduces the background of the TOC problem, providing a foundation for the subsequent discussions. In Section 3, the derivation of the FNTD algorithm is presented, utilizing the isochronic region (IR) method. Section 4 offers a practical rule for adjusting the parameters of FNTD based on frequency-sweep testing. In Section 5, a comparative analysis is conducted to demonstrate the superiority of FNTD in terms of convergence speed, tracking performance, differentiation accuracy, and filtering capabilities when compared to other tracking differentiators. Finally, Section 6 summarizes the key findings and contributions of this paper.

2. TOC problem description

In this section, we review some fundamental concepts related to the TOC problem. This is crucial for understanding the theoretical foundation of the tracking differentiator algorithms that will be discussed later in the paper.

The first-order high-pass filter, often employed as a classical differentiator in servo control systems, has a transfer function that characterizes its response to input signals. The output of the differentiator can be expressed as

$$y = w(s)v = \frac{s}{Ts+1}v = \frac{1}{T}(1 - \frac{1}{Ts+1})v \tag{2.1}$$

where T represents a relatively small time constant, v denotes the input to the differential system, y is the system output, and $w(s)$ represents the transfer function. Equation (2.1) can be rewritten as

$$y = \frac{1}{T}(v - \frac{v}{Ts+1}) \tag{2.2}$$

Define $\frac{v}{Ts+1}$ as the differential signal $v'(t)$, then

$$y(t) = \frac{1}{T}(v(t) - v^{'}(t)) \tag{2.3}$$

According to the definition of derivative, we have

$$v^{'}(t) \approx v(t-T) \tag{2.4}$$

From (2.3) and (2.4), we have

$$y(t) \approx \frac{1}{T} * (v(t) - v(t-T)) \approx \dot{v}(t) \tag{2.5}$$

and when the time constant T is smaller, the output signal y gets closer to the differential signal $v^{'}(t)$.

Assuming that the measured signal is only coupled with the random noise signal $r(t)$, from (2.5) we have

$$y(t) = \frac{1}{T}(v(t) + r(t) - (v^{'}(t) + r^{'}(t))) \tag{2.6}$$

which satisfies the following equation:

$$\frac{dy}{dt} = -\frac{1}{T}(y - (v(t) + r(t))) \tag{2.7}$$

The solution to the above differential equation is

$$y(t) = \dot{v}(t) + \frac{1}{T}r(t) \tag{2.8}$$

From (2.8), the noise in the signal is amplified by $1/T$. In order to eliminate or reduce the noise amplification effect, the above equation can be rewritten as

$$v(t) \approx \frac{v(t-\tau_1) - v(t-\tau_2)}{\tau_2 - \tau_1}, 0 < \tau_1 < \tau_2 \tag{2.9}$$

The time constants of the two inertial links are denoted by τ_1 and τ_2. The transfer function corresponding to the above equation is

$$y = \frac{s}{\tau_1\tau_2 s^2 + (\tau_1 + \tau_2)s + 1}v \tag{2.10}$$

The equivalent state space realization of (2.10) is

$$\begin{cases} x_1 = x_2 \\ x_2 = -\dfrac{1}{\tau_1\tau_2}\Big(x_1 - v(t)\Big) - \dfrac{\tau_1 + \tau_2}{\tau_1\tau_2}x_2 \\ y_3 = x_2 \end{cases} \tag{2.11}$$

where x_1 and x_2 are the state variables and y is the output variable. Equation (2.11) can be rewritten as the following general form [1]:

$$\begin{cases} \dot{x_1} = x_2 \\ \dot{x_2} = f(x_1 - v(t), x_2) \end{cases} \tag{2.12}$$

When the above differential equation has a solution, it is guaranteed that x_1 converges to $v(t)$ and x_2 converges to $\dot{v}(t)$, then (2.12) constitutes a differentiator. It was the desire to find a differentiator that gave birth to the time-optimal control based tracking differentiator as presented in the following.

The double-integral system is defined as

$$\begin{cases} \dot{x}_1 = x_2, \\ \dot{x}_2 = u, \end{cases} \quad |u| \le r \tag{2.13}$$

where u is the control signal and r is a constant constraint of the control input.

The task of finding a control law that steers any initial state $[x_1(0), x_2(0)]$ of a system (2.13) to the origin in the shortest possible time is known as the TOC problem. Solving this problem involves determining the optimal control strategy that minimizes the time required for the system to reach its destination.

The solution to this problem is [33–35]

$$u(t) = -r\text{sign}(s) \tag{2.14}$$

where the switching function s is

$$s = \begin{cases} x_1(t) + \frac{x_2(t)|x_2(t)|}{2r} & x_1(t) + \frac{x_2(t)|x_2(t)|}{2r} \neq 0 \\ x_2(t) & x_1(t) + \frac{x_2(t)|x_2(t)|}{2r} = 0, x(t) \neq 0 \\ 0 & x_1(t) + \frac{x_2(t)|x_2(t)|}{2r} = 0, x(t) = 0 \end{cases} \tag{2.15}$$

Substitute $x_1(t)$ with $x_1(t) - v(t)$ and $x_2(t)$ with $x_2(t) - \dot{v}(t)$, respectively, in (2.15), which is easily extended to a tracking problem as follows:

$$s = \begin{cases} x_1(t) - v(t) + \frac{x_2(t)|x_2(t)|}{2r} & x_1(t) - v(t) + \frac{(x_2(t)-\dot{v}(t))|x_2(t)-\dot{v}(t)|}{2r} \neq 0 \\ x_2(t) & x_1(t) - v(t) + \frac{(x_2(t)-\dot{v}(t))|x_2(t)-\dot{v}(t)|}{2r} = 0, x(t) \neq 0 \\ 0 & x_1(t) - v(t) + \frac{(x_2(t)-\dot{v}(t))|x_2(t)-\dot{v}(t)|}{2r} = 0, x(t) = 0 \end{cases} \tag{2.16}$$

where $v(t)$ and $\dot{v}(t)$ are the desired state trajectory and its derivative. Note that the conditions $x(t) = 0$ and $x_1(t) + \frac{x_2(t)|x_2(t)|}{2r} = 0$ are hard to achieve in the noisy environment.

Remark 2.1. *From (2.8), the noise in the original signal could be amplified by 1/T. To reduce the noise amplification effect, it is proposed here that a tracking differentiator can be designed which guarantees that x_1 converges to $v(t)$ and x_2 converges to $\dot{v}(t)$. The issue of extracting the differential information of real signals is first transformed into designing a rapid TD problem, then it is reduced to solving the problem of the TOC issue in the shortest time.*

3. FNTD algorithm design

Given that the majority of control algorithms are nowadays implemented in the discrete-time domain, there is a desire to identify the TOC law for a discrete-time double-integrator plant, aiming to construct a TD. This problem, referred to as the discrete-time optimal control (DTOC) problem, was first proposed by Han [1]. However, directly discretizing the solution from continuous TOC can be problematic due to high-frequency chattering in the control signals.

In this section, the construction of a FNTD based on the hyperbolic tangent function is proposed by the IR method. The FNTD algorithm is a discrete time closed-form solution to the TOC problem.

For a discrete-time double-integral system

$$x(k+1) = Ax(k) + Bu(k), |u(k)| \leq r \tag{3.1}$$

where $A = \begin{bmatrix} 1 & h \\ 0 & 1 \end{bmatrix}$, $B = \begin{bmatrix} 0 \\ h \end{bmatrix}$, and h is the sampling period, $x(k) = [x_1(k), x_2(k)]^T$.

Definition 3.1. *(DTOC Problem). For the system* (3.1) *and its initial state $x(0)$, there exists at least one control sequence $u(k^*)$, $|u(k)| \leq r$, $k \leq N$, such that $k^* = \min\{k|x(k) = 0\}$, where N is a finite number.*

Definition 3.2. *(IR $G(k)$). For any $x(0) \in G(k)$, $\exists u(0), u(1), \ldots, u(k)$ makes the solution of* (3.1) *satisfy $x(k) = 0$.*

Remark 3.1. *The whole phase plane is divided into two regions $G(k)$ and $R^2 - G(k)$.*

Proof. For a DTOC problem, we need to find the control sequence $u(0), u(1), \ldots, u(k)$ that makes $x(k) = 0$ for any $x(0)$. The proof is divided into two parts:

(i) Determine $G(k)$.

(ii) $\forall x(0) \in G(k)$ and $\forall x(0) \notin G(k)$; find the function of $u(k)$ that satisfies $x(k) = 0$.

To begin, examine $G(k)$. For (3.1), we have the iteration formula of $x(k)$

$$x(k) = A^k x(0) + A^{k-1}Bu(0) + \ldots + ABu(k-2) + Bu(k-1) \tag{3.2}$$

For $x(k)$=0, we can solve $x(0)$

$$x(0) = -A^{-1}Bu(0) - A^{-2}Bu(1) - \ldots A^{-k}Bu(k-1) \tag{3.3}$$

With $A^{-k} = \begin{bmatrix} 1 & -kh \\ 0 & 1 \end{bmatrix}$, (3.3) can be rewritten as

$$x(0) = \sum_{i=1}^{k} \begin{bmatrix} ih^2 \\ -h \end{bmatrix} u(i-1) \tag{3.4}$$

So, the IR $G(k)$ is

$$G(k) = \sum_{i=1}^{k} \begin{bmatrix} ih^2 \\ -h \end{bmatrix} u(i-1), |u(i) \le r| \tag{3.5}$$

Case 1: When $x(0) \in G(1)$. From (3.5), we have

$$G(1) = \begin{bmatrix} h^2 \\ -h \end{bmatrix} u(0) \tag{3.6}$$

that is, $G(1)$ is a line that satisfies $x_1(0) + hx_2(0) = 0, |x_2(0)| \le hr$. As shown in Figure 1, $G(1)$ is a line connecting a_1 and a_{-1}.

When $x(0) \in G(1)$, the time optimal control law is [24]

$$u(0) = -\frac{x_2(0)}{h}, |x_2(0)| \le hr, x_1(0) + hx_2(0) = 0 \tag{3.7}$$

Case 2: When $x(0) \in \{x \mid (x \notin G(1)) \cap (x_1 + hx_2 = 0)\}$

In this region, x(0) is still on the same line of $G(1)$ but goes beyond points a_1,a_{-1}. The corresponding control signal is [24] $u(0) = -r\text{sign}(x_2(0) - hr)$ until $x(0)$ enters $G(1)$. Here, using the hyperbolic tangent function to transition to extreme value [36], we have

$$u(0) = -r\tanh(\alpha(x_2(0) - hr)), |x_2(0)| \ge hr, \alpha \in \mathbb{R}^+ \tag{3.8}$$

where α is a constant; when α is larger, the hyperbolic tangent function is closer to the sign function; and u approaches the extreme value faster. Additionally, from (3.8), when x(0) is closer to the boundary curve, u will decrease.

Case 3: When $x(0) \in G(2)$.

From (3.5), we have

$$G(2) = \begin{bmatrix} h^2 \\ -h \end{bmatrix} u(0) + \begin{bmatrix} 2h^2 \\ -h \end{bmatrix} u(1) \tag{3.9}$$

as shown in Figure1.

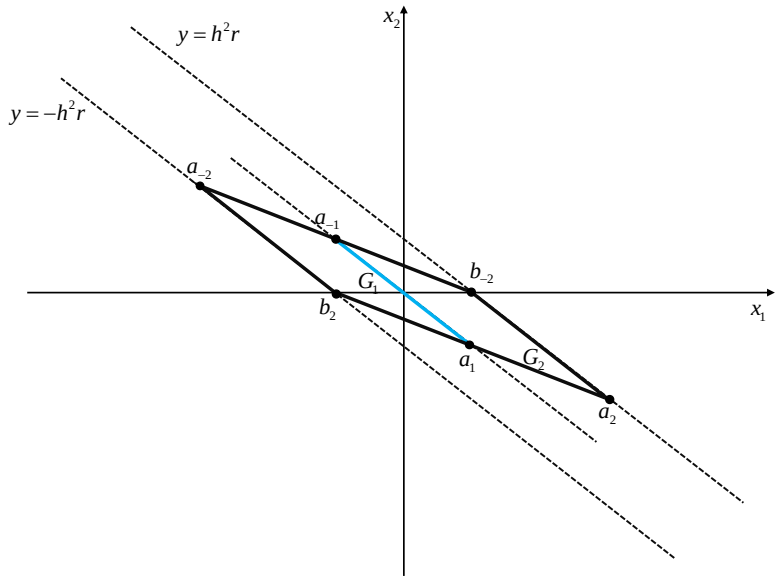

Figure 1. Illustration of $G(1)$ and $G(2)$.

Let

$$y = x_1 + hx_2 \tag{3.10}$$

Then, the boundaries of G_2 are the following four straight lines:

$$\begin{cases} a_2b_{-2} : y = h^2 r \\ a_{-2}b_2 : y = -h^2 r \\ a_{-2}b_{-2} : y + hx_2 = h^2 r \\ a_2b_{-2} : y + hx_2 = -h^2 r \end{cases} \tag{3.11}$$

When $x(0) \in G(2)$, the TOC law is [24]

$$u(0) = -\frac{x_2(0) + y/h}{h}, |x_2 + \frac{y}{h}| \le hr, |y| \le h^2 r \tag{3.12}$$

Case 4: When $x(0) \in \{x \mid (x \notin G(2)) \cap (|y| \le h^2 r)\}$

In this region, x(0) is not $G(2)$, but it is still on the area surrounded by two parallel lines a_2b_{-2}, $a_{-2}b_2$. Here, u uses the hyperbolic tangent function to transition to the extreme value, that is,

$$u = -r\tanh(\alpha(x_2 + \frac{y}{h})), |x_2 + \frac{y}{h}| > hr, |y| \le h^2 r, \alpha \in \mathbb{R}^+ \tag{3.13}$$

Case 5: When $x(0) \in \{x \mid |y| \ge h^2 r\}$

In this region, x_0 is located outside the parallel line a_2b_{-2}, $a_{-2}b_2$.

From (3.5), the broken line a_k, a_{-k}, b_k, b_{-k} is defined as

$$a_k = \left\{ \sum_{i=1}^{k} \begin{bmatrix} ih^2 \\ -h \end{bmatrix} u(i-1), u(i) = r \right\} \tag{3.14}$$

$$a_{-k} = \left\{ \sum_{i=1}^{k} \begin{bmatrix} ih^2 \\ -h \end{bmatrix} u(i-1), u(i) = -r \right\} \tag{3.15}$$

$$b_k = \left\{ \sum_{i=1}^{k} \begin{bmatrix} ih^2 \\ -h \end{bmatrix} u(i-1), u(0) = r, u(i) = -r \text{ for } i > 0 \right\} \tag{3.16}$$

$$b_{-k} = \left\{ \sum_{i=1}^{k} \begin{bmatrix} ih^2 \\ -h \end{bmatrix} u(i-1), u(0) = -r, u(i) = r \text{ for } i > 0 \right\} \tag{3.17}$$

Here, Γ_0^+ is defined as the boundary curve formed by connecting $\ldots, a_k, a_{k-1}, \ldots, a_2, b_2, \ldots, b_{k-1}, b_k, \ldots$, and Γ_0^- is defined as the boundary curve formed by connecting $\ldots, b_{-k}, b_{-(k-1)}, \ldots, b_{-2}, a_{-2}, \ldots, a_{-(k-1)}, a_{-k}, \ldots$. Zhang [28] rewrote the function of Γ_0^+ and Γ_0^- together as Γ^0 as follows:

$$\Gamma^0(x_1, x_2, r, h) = x_2 + \frac{1}{2}(\sqrt{h^2r^2 + 8r|y|} - hr)\text{sign}(y), |y| \geq h^2 r \tag{3.18}$$

where $\Gamma^0 = -hr$ is the curve Γ_0^-, and $\Gamma^0 = hr$ is the curve Γ_0^+.

Using the hyperbolic tangent function to substitute the sign function, we have

$$\Gamma(x_1, x_2, r, h, \alpha) = x_2 + \frac{1}{2}(\sqrt{h^2r^2 + 8r|y|} - hr)\tanh(\alpha y), |y| \geq h^2 r, \alpha \in \mathbb{R}^+ \tag{3.19}$$

The boundary curves Γ_0 and Γ are shown in Figure 2.

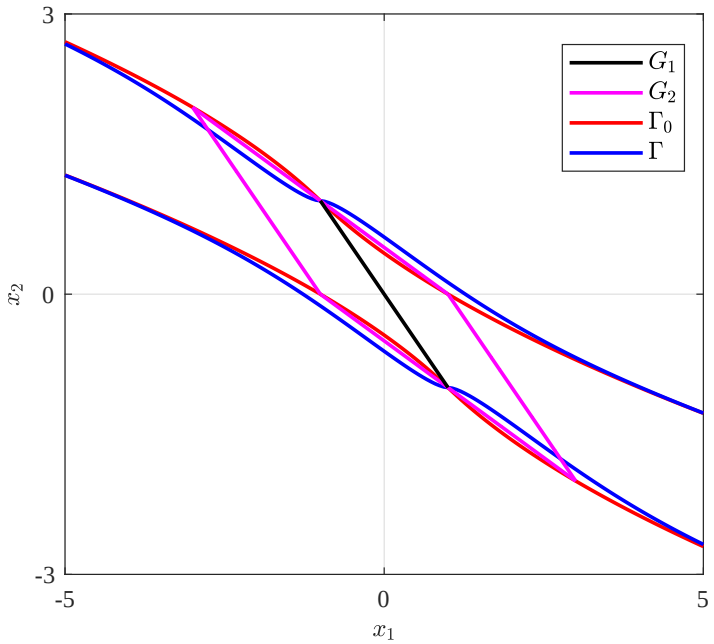

Figure 2. Illustration of $G(1)$, $G(2)$, Γ_0 and Γ.

Note that the region surrounded by the boundary curve Γ is misaligned with the $G(2)$, but (3.19) is valid on the region $|y| \geq h^2 r$. So, the phase plane $|y| \geq h^2 r$ is divided into the following two parts:

$$\begin{cases} |\Gamma(x_1, x_2, r, h)| \leq hr, & x = [x_1, x_2]^T \text{ is in the region surrounded by } \Gamma \\ |\Gamma(x_1, x_2, r, h)| \geq hr, & x = [x_1, x_2]^T \text{ is outside the region surrounded by } \Gamma \end{cases} \tag{3.20}$$

According to [24], when $x(0) \in \{x \mid |y| \geq h^2 r\}$, the control signal is

$$u = \begin{cases} -r\text{sign}(\Gamma), |\Gamma| > \text{hr} \\ -r\frac{\Gamma}{hr}, |\Gamma| \leq hr \end{cases} \tag{3.21}$$

Combining (3.12), (3.13), and (3.21), we redefine $\Gamma(x_1, x_2, r, h)$ as

$$\Gamma(x_1, x_2, r, h, \alpha) = \begin{cases} x_2 + \frac{\left(\sqrt{h^2r^2+8r|y|}-hr\right)}{2}\tanh(\alpha y), |y| > h^2 r \\ x_2 + y/h, |y| \leq h^2 r, \alpha \in \mathbb{R}^+ \end{cases} \tag{3.22}$$

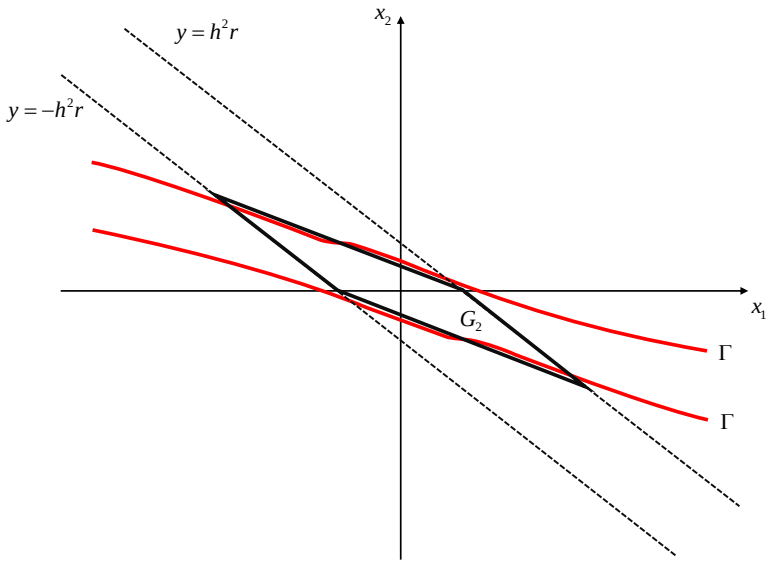

Figure 3. Illustration of $G(2)$ and Γ.

The characteristic curves $G(2)$ and Γ of the FNTD algorithm are shown in Figure 3. The complete FNTD algorithm based on the hyperbolic tangent function coded in a digital computer is as follows:

$$\begin{cases} u = fntd(x_1, x_2, r, h, \alpha) \\ d = rh \\ d_0 = hd \\ y = x_1 + hx_2 \\ \Gamma_0 = \sqrt{d^2 + 8r|y|} \\ \Gamma = \begin{cases} x_2 + \dfrac{(\Gamma_0 - d)}{2}\tanh(\alpha y), |y| > d_0 \\ x_2 + \dfrac{y}{h}, |y| \leq d_0 \end{cases} \\ fntd(x_1, x_2, r, h, \alpha) = -\begin{cases} r\tanh(\alpha\Gamma), |\Gamma| > d \\ r\dfrac{\Gamma}{d}, |\Gamma| \leq d \end{cases} \end{cases} \tag{3.23}$$

Changing two adjustable parameters α in (3.23) into independent new variables α_1, α_2, we rewrite the FNTD algorithm in a new form,

$$\begin{cases} u = fntd(x_1, x_2, r, h, \alpha_1, \alpha_2) \\ d = rh \\ d_0 = hd \\ y = x_1 + hx_2 \\ \Gamma_0 = \sqrt{d^2 + 8r|y|} \\ \Gamma = \begin{cases} x_2 + \dfrac{(\Gamma_0 - d)}{2} \tanh(\alpha_1 y), |y| > d_0 \\ x_2 + \dfrac{y}{h}, |y| \le d_0 \end{cases} \\ fntd(x_1, x_2, r, h, \alpha_1, \alpha_2) = -\begin{cases} r\tanh(\alpha_2\Gamma), |\Gamma| > d \\ r\dfrac{\Gamma}{d}, |\Gamma| \le d \end{cases} \end{cases} \tag{3.24}$$

where x_1 is the desired trajectory, x_2 is its derivative, h is the filtering factor, and r is the speed factor [1, 23].

Remark 3.2. *The tunable parameter α_1 primarily influences the shape of the boundary curve, while α_1, α_2 jointly modify the control law, thereby altering the tracking speed of the signal.*

4. Frequency-domain characteristics analysis

Given a reference signal sequence $v(k), k = 0, 1, 2, \ldots$, the FNTD algorithm based on (3.24) can be constructed as

$$\begin{cases} u(k) = fntd(x_1(k) - v(k), x_2(k), r, h, \alpha_1, \alpha_2) \\ x_1(k+1) = x_1(k) + Tx_2(k) \\ x_2(k+1) = x_2(k) + Tu(k), |u(k)| \le r, k = 0, 1, 2, ... \end{cases} \tag{4.1}$$

The objective of this section is to show how damping factors α_1, α_2 affect the outputs of TD in the frequency domain. For different α_1 and α_2, we use the method of the frequency-sweep test to get the Bode diagram and analyze frequency domain characteristics of FNTD.

Here, to test the frequency domain characteristics of FNTD under ideal conditions, the sinusoidal signal input does not contain any random noise. $T = 0.001, h = 0.001, r = 100$, and five groups of α_1, α_2 are set as follows: $[\alpha_1, \alpha_2] = [1, 1], [2, 1], [100, 1], [1, 10], [1, 100]$. The input signal is $v(t) = \sin(2\pi ft)$, where f ranges from 0.1Hz to 10Hz with a time step of 0.01 Hz. For each frequency point, we run 20,000 samples and record the data in the sampling interval [10001, 15000]. The simulation test results of the amplitude-frequency and phase-frequency curves of the proposed TD are shown in Figures 4 and 5.

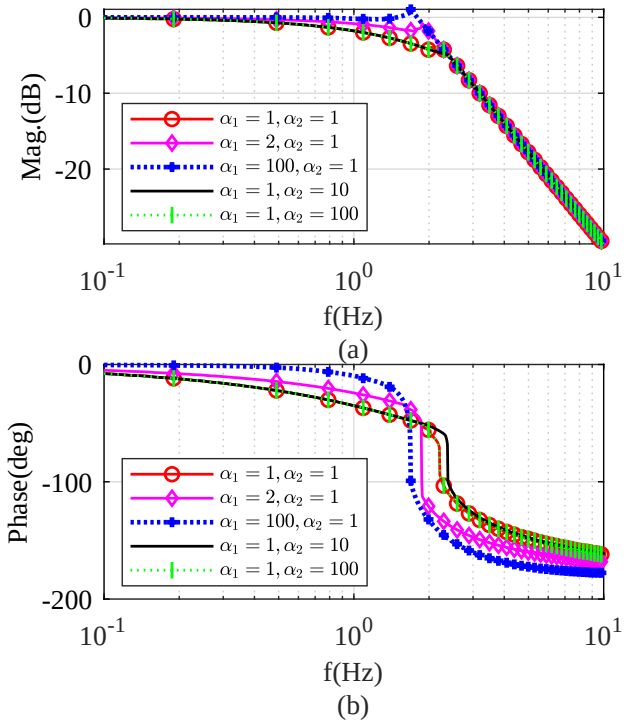

Figure 4. Frequency-domain characteristics of output x_1. (a) Amplitude-frequency characteristics; (b) Phase-frequency characteristics.

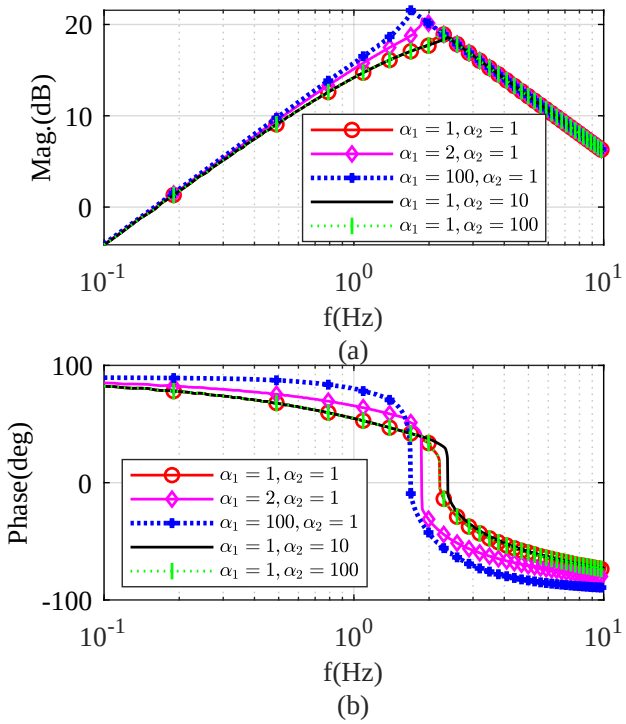

Figure 5. Frequency-domain characteristics of output x_2. (a) Amplitude-frequency characteristics; (b) Phase-frequency characteristics.

From Figure 4, the amplitude-frequency characteristic of the tracking signal approximates an ideal first-order low-pass filter. When $\alpha_2 = 1$ and α_1 increases from 1 to 100, the cutoff frequency also increases. The FNTD can track the higher frequency of the input signal, and the corresponding amplitude-frequency characteristic moves right. However, after exceeding the cutoff frequency, the phase of the input signal quickly decreases to -180°. When $\alpha_1 = 1$, altering α_2 has little effect on the amplitude-frequency characteristic curve.

In Figure 5, the phase-frequency characteristic of the differential signal approximates a band-pass filter. Before the turning frequency, the phase almost remains 90° ahead. However, the phase quickly decreases to -90° near the cutoff frequency. When $\alpha_2 = 1$ and α_1 increases from 1 to 100, the filtering ability of differential signals against high-frequency noise is enhanced.

Remark 4.1. *From Figures 4 and 5, a bigger α_1 enables the improvement of the quality of amplitude-frequency characteristics, and we can see that the boundary curve has a great impact on the speed of the signal tracking combined* (3.24)*. Considering the properties of tanh(αy), as α increases, tanh(αy) approaches 1 from 0 more quickly.*

We suggest increasing the parameters α_1 and α_2 as much as possible to achieve a better control law as shown below:

$$\begin{cases} \alpha_1 \geq 100 \\ \alpha_2 \geq 100 \end{cases} \tag{4.2}$$

This approach will yield improved simulation results when utilizing the proposed algorithm.

5. Simulation analysis

To verify the effectiveness of the proposed FNTD, in this section, we present simulations comparing FNTD (denoted as TD_0) with the following three differentiators in terms of convergence and filtering characteristics.

TD_1: The classical differentiator [37]

$$\begin{cases} \dot{x}_1 = x_2 \\ \dot{x}_2 = \frac{1}{\tau_1\tau_2}\left(-(x_1 - v(t)) - \frac{\tau_1+\tau_2}{\tau_1\tau_2}x_2\right) \end{cases}$$

where τ_1 and τ_2 are tuning parameters.

TD_2: The nonlinear differentiator [12]

$$\begin{cases} \dot{x}_1 = x_2 \\ \dot{x}_2 = R^2\left(- a_0(x_1 - v(t)) - a_1(x_1 - v(t))^{\frac{m}{n}} - b_0\frac{x_2}{R} - b_1\left(\frac{x_2}{R}\right)^{\frac{m}{n}} \right) \end{cases}$$

where the parameters $R, a_0, a_1, b_0, b_1 > 0, m, n > 0$ are tunable odd numbers.

TD_3: Robust exact differentiator using the sliding-mode technique [20]

$$\begin{cases} \dot{x}_1 = x_2 - \alpha|x_1 - v|^{0.5}\,\mathrm{sign}(x_1 - v) \\ \dot{x}_2 = -\beta\,\mathrm{sign}(x_1 - v) \end{cases}$$

where α and β are tunable parameters.

We use the Euler method to discretize the state space. In all simulations, we choose the initial state $[x_1(0), x_2(0)] = [-1, 1]$ and the sampling period $T = 0.01$. All parameters are determined by the trial and error method, which are presented in Table 1.

Table 1. Parameters of four kinds of TDs.

TD	parameters
TD_0	$h = 0.26, r = 1, \alpha_1 = 100, \alpha_2 = 100$
TD_1	$\tau_1 = 0.81, \tau_2 = 1.5$
TD_2	$R = 25, a_0 = 0.089, a_1 = 0.00001, b_0 = 1.93, b_1 = 0.00015, m = 8.1, n = 9$
TD_3	$\alpha = 3.7997, \beta = 0.315$

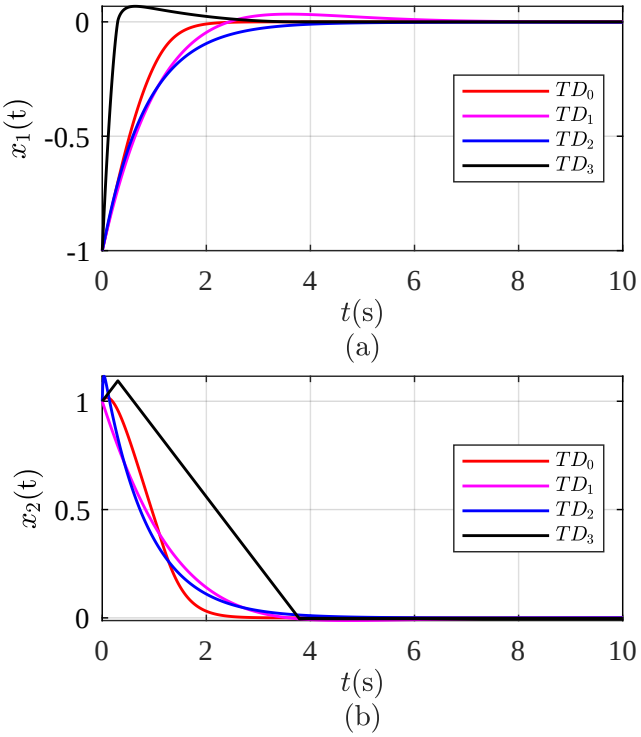

Figure 6. Comparison of the convergence of four TD algorithms. (a) signal-tracking x_1; (b) differentiation acquisition x_2.

Table 2. Comparison of convergence of x_1 for four TDs.

TD	adjusting time	overshoot	steady state error
TD_0	2 s	0	0
TD_1	2.4 s	3.4%	0
TD_2	4 s	0	0.1%
TD_3	3.2 s	6.8%	0

The state trajectories of four differentiators are shown in Figure 6. Additionally, we calculate the

convergence performance indicators of the four differentiators, as shown in Tables 2 and 3. Compared with other differentiators, the system with FNTD has the shortest adjusting time and smallest overshoot, which optimally drives the initial condition to the origin.

Table 3. Comparison of convergence of x_2 for four TDs.

TD	adjusting time	overshoot
TD_0	2.5 s	0
TD_1	3.5 s	1.2%
TD_2	4 s	11.5%
TD_3	3.8 s	9.5%

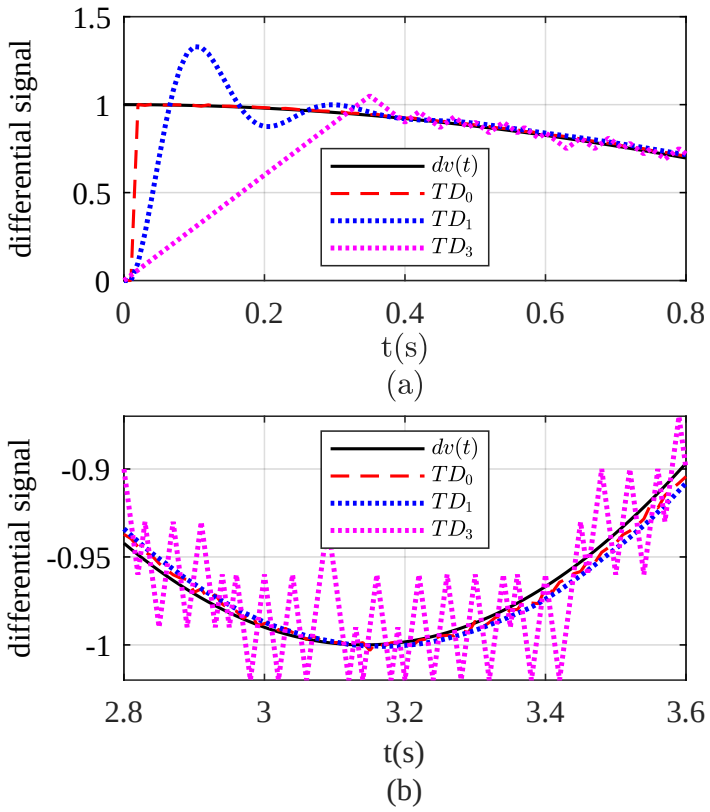

Figure 7. Comparisons of differentiation acquisition when SNR = 100 dB. (a) the transient process. (b) the steady process.

Table 4. Parameters of three kinds of TDs.

TD	parameters
TD_0	$h = 0.01, r = 230, \alpha_1 = 100, \alpha_2 = 100$
TD_1	$1/(\tau_1 * \tau_2) = 1000, (\tau 1 + \tau 2)/(\tau 1 * \tau 2) = 0.03$
TD_3	$\alpha = 3, \beta = 3$

In practical engineering, TD_1 and TD_3 are commonly used, which are compared with TD_0(FNTD) to verify the filtering performance of the proposed TD algorithm. We choose the input signal $v(t)$=

awgn(sin(*t*), SNR), where the function *awgn* (additive white Gaussian noise) in Matlab adds white Gaussian noise to the signal. Suppose the initial state is $[x_1(0), x_2(0)] = [0, 0]$ and the sampling period is $T = 0.01$. All parameters of three kinds of TDs are shown in Table 4. To ensure that the differential signal has sufficient noise suppression performance, the simulation results with different signal-to-noise ratio (SNR) of Gaussian noise are shown in Figures 7 and 8.

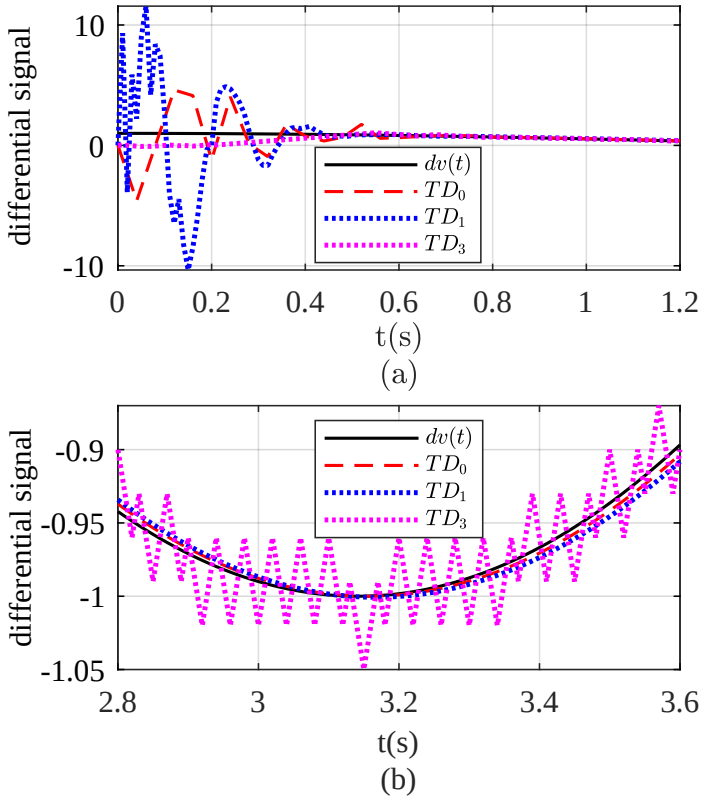

Figure 8. Comparisons of differentiation acquisition when SNR = 100*t* dB. (a) the transient process. (b) the steady process.

When SNR = 100 dB, the transient and steady processes are shown in Figure 7. From Figure 7, it can be seen that all algorithms have a certain level of noise suppression ability, but compared to TD_0 and TD_1, TD_3 exhibits a more violent oscillation response. In Figure 7(a), FNTD exhibits the fastest response speed and the smallest overshoot among the three TD algorithms. TD_1 has superior speed, but with the greatest overshoot. On the other hand, while TD_3 displays smaller overshoot, its response speed is the slowest, as shown in Table 5. During the steady process in Figure 7(b), TD_0 has the shortest tracking phase delay compared with TD_1 and D_3.

Table 5. Comparison of dynamic performance of differential signals for three TD algorithms during transient processes when SNR = 100 dB.

TD	adjusting time	overshoot
TD_0	0.02 s	0
TD_1	0.25 s	33%
TD_3	0.42 s	10%

From Figure 8(a), when SNR = 100t dB, during the transient process phase, TD_3 has the smallest overshoot and chattering; TD_0 is the next, and TD_1 has the largest. In Figure 8(b), TD_0 is most accurate in tracking and differentiation compared with TD_1 and TD_3 in steady process.

Remark 5.1. *In Figure 8, a performance comparison simulation experiment of the three differentiators has been conducted by gradually increasing the SNR. (1) Under low SNR conditions. When SNR ≤ 35 dB, as shown in Figure 8(a), TD_0 and TD_1 exhibit overshoot and long transient time, using the same parameters as those for SNR = 100 dB during the transient process. (2) Under high SNR conditions. From Figure 8(b), it is evident that the three TD algorithms all demonstrate parameter adaptability in high SNR noise, as seen in Figure 7(b), but among three TD algorithms, TD_0 is the smoothest and most accurate in capturing differential signals, making it more suitable for capturing actual differential signals in higher SNR noise environments.*

In summary, through the performance comparison in various scenarios such as the transition process and steady-state process under different noise conditions, the FNTD has achieved superior noise filtering and differential extraction effects compared to other differentiators.

6. Conclusions

To quickly extract accurate differential signals from contaminated signals, a FNTD algorithm based on the hyperbolic tangent function is proposed in this paper. To begin, the differential extraction problem is transformed into a double integral system based on TOC law. Next, using the equal time zone (IR) method in the discrete time domain, a FNTD algorithm based on the hyperbolic tangent function is proposed. Then, the frequency domain characteristics of FNTD are analyzed, and the adjustment rules of parameters are given by the frequency scanning test method. Finally, the simulation results show that the proposed FNTD has fast and accurate tracking performance, and has excellent filtering and differential extraction abilities compared with other differentiators.

Future work includes the phase delay compensation algorithm and DTOC-based TD design suitable for engineering applications.

Use of AI tools declaration

The authors declare they have not used Artificial Intelligence (AI) tools in the creation of this article.

Acknowledgments

This work was supported by the National Natural Science Foundation of China (61304036)) and Key Laboratory of Cross-Domain Flight Interdisciplinary Technology (2024-KF01007) .

Conflict of interest

The authors declare there is no conflicts of interest.

References

1. J. Han, From pid to active disturbance rejection control, *IEEE Trans. Ind. Electron.*, **56** (2009), 900–906. https://doi.org/10.1109/TIE.2008.2011621
2. H. Ríos, E. Punta, L. Fridman, Fault detection and isolation for nonlinear non-affine uncertain systems via sliding-mode techniques, *Int. J. Control*, **90** (2017), 218–230. https://doi.org/10.1080/00207179.2016.1173727
3. C. Vázquez, S. Aranovskiy, L. B. Freidovich, L. M. Fridman, Time-varying gain differentiator: A mobile hydraulic system case study, *IEEE Trans. Control Syst. Technol.*, **24** (2016), 1740–1750. https://doi.org/10.1109/TCST.2015.2512880
4. W. Ji, D. Lv, S. Luo, Y. Sun, Multiple models-based fault tolerant control of levitation module of maglev vehicles against partial actuator failures, *IEEE Trans. Veh. Technol.*, **2024** (2024). https://doi.org/10.1109/TVT.2024.3399235
5. H. Zhang, G. Xiao, Y. Xie, W. Guo, C. Zhai, *Tracking Differentiator Algorithms*, Springer, 2021. https://doi.org/10.1007/978-981-15-9384-0
6. R. P. Borase, D. Maghade, S. Sondkar, S. Pawar, A review of pid control, tuning methods and applications, *Int. J. Dyn. Control*, **9** (2021), 818–827. https://doi.org/10.1007/s40435-020-00665-4
7. H. Zhang, G. Xiao, Y. Xie, W. Guo, C. Zhai, H. Zhang, et al., Tracking differentiators in real-life engineering, in *Tracking Differentiator Algorithms. Lecture Notes in Electrical Engineering*, **717** (2021), 77–90. https://doi.org/10.1007/978-981-15-9384-0_7
8. H. Feng, S. Li, A tracking differentiator based on taylor expansion, *Appl. Math. Lett.*, **26** (2013), 735–740. https://doi.org/10.1016/j.aml.2013.02.003
9. H. Wu, J. Huang, Control of induction motor drive based on adrc and inertia estimation, in *2019 IEEE International Electric Machines and Drives Conference (IEMDC)*, IEEE, (2019), 1607–1612. https://doi.org/10.1109/IEMDC.2019.8785393
10. A. Levant, X. Yu, Sliding-mode-based differentiation and filtering, *IEEE Trans. Autom. Control*, **63** (2018), 3061–3067. https://doi.org/10.1109/TAC.2018.2797218
11. A. Levant, M. Livne, X. Yu, Sliding-mode-based differentiation and its application, *IFAC-PapersOnLine*, **50** (2017), 1699–1704. https://doi.org/10.1016/j.ifacol.2017.08.495
12. W. Bai, W. Xue, Y. Huang, H. Fang, On extended state based kalman filter design for a class of nonlinear time-varying uncertain systems, *Sci. China Inf. Sci.*, **61** (2018), 1–16. https://doi.org/10.1007/s11432-017-9242-8
13. J. Yu, S. Jin, Sliding mode tracking differentiator with adaptive gains for filtering and derivative estimation of noisy signals, *IEEE Access*, **9** (2021), 86017–86024. https://doi.org/10.1109/ACCESS.2021.3088544
14. Y. Liu, L. Hao, Adaptive tracking differentiator control for nonlinear stochastic systems, in *2022 13th Asian Control Conference (ASCC)*, (2022), 512–517. https://doi.org/10.23919/ASCC56756.2022.9828327

15. H. Zhang, Y. Xie, G. Xiao, C. Zhai, Z. Long, A simple discrete-time tracking differentiator and its application to speed and position detection system for a maglev train, *IEEE Trans. Control Syst. Technol.*, **27** (2018), 1728–1734. https://doi.org/10.1109/TCST.2018.2832139

16. X. Wang, S. Jin, High-order sliding mode tracking differentiator with neural network based adaptive parameter estimation, in *Journal of Physics: Conference Series*, **2613** (2023), 012013. https://doi.org/10.1088/1742-6596/2613/1/012013

17. Y. Feng, Z. Li, Y. Liu, Z. He, H. Li, Differentiator-based adaptive h∞ tracking control of fully actuated systems, in *2024 3rd Conference on Fully Actuated System Theory and Applications (FASTA)*, IEEE, (2024), 680–684. https://doi.org/10.1109/FASTA61401.2024.10595180

18. A. M. Dabroom, H. K. Khalil, Output feedback sampled-data control of nonlinear systems using high-gain observers, *IEEE Trans. Autom. Control*, **46** (2001), 1712–1725. https://doi.org/10.1109/9.964682

19. X. Wang, Z. Chen, Z. Yuan, Design and analysis for new discrete tracking-differentiators, *Appl. Math. J. Chin. Univ.*, **18** (2003), 214–222. https://doi.org/10.1007/s11766-003-0027-0

20. A. Levant, Robust exact differentiation via sliding mode technique, *Automatica*, **34** (1998), 379–384. https://doi.org/10.1016/S0005-1098(97)00209-4

21. A. Abdessameud, A. Tayebi, Global trajectory tracking control of vtol-uavs without linear velocity measurements, *Automatica*, **46** (2010), 1053–1059. https://doi.org/10.1016/j.automatica.2010.03.010

22. L. Zhang, Z. Zhang, L. Huang, Hybrid non-linear differentiator design for a permanent-electro magnetic suspension maglev system, *IET Signal Process.*, **6** (2012), 559–567. https://doi.org/10.1049/iet-spr.2011.0264

23. J. Han, L. Yuan, The discrete form of tracking-differentiator, *J. Syst. Sci. Math. Sci.*, **19** (1999), 263–273. https://doi.org/10.12341/jssms09882

24. Z. Gao, On discrete time optimal control: A closed-form solution, in *Proceedings of the 2004 American Control Conference*, IEEE, **1** (2004), 52–58. https://doi.org/10.23919/ACC.2004.1383578

25. Z. Lu, S. Bai, M. Jiang, Y. Xu, F. Liu, Improved design of linear self-turbulent permanent magnet synchronous motor speed controller, *J. Electron. Meas. Instrum.*, **36** (2023), 73–81.

26. Z. Hao, Y. Yang, Y. Gong, Z. Hao, C. Zhang, H. Song, et al., Linear/nonlinear active disturbance rejection switching control for permanent magnet synchronous motors, *IEEE Trans. Power Electron.*, **36** (2021), 9334–9347. https://doi.org/10.1109/TPEL.2021.3055143

27. J. Li, H. Ren, Y. Zhong, Robust speed control of induction motor drives using first-order auto-disturbance rejection controllers, *IEEE Trans. Ind. Appl.*, **51** (2014), 712–720. https://doi.org/10.1109/TIA.2014.2330062

28. H. Zhang, G. Xiao, X. Yu, Y. Xie, On convergence performance of discrete-time optimal control based tracking differentiator, *IEEE Trans. Ind. Electron.*, **68** (2020), 3359–3369. https://doi.org/10.1109/TIE.2020.2979530

29. L. Zhao, H. Cheng, J. Zhang, Y. Xia, Angle attitude control for a 2-dof parallel mechanism of pmas using tracking differentiators, *IEEE Trans. Ind. Electron.*, **66** (2018), 8659–8669. https://doi.org/10.1109/TIE.2018.2884215

30. Y. Xie, Y. Li, L. She, P. Cui, C. Dai, A discrete second-order nonlinear tracking-differentiator based on boundary characteristic curves, *Inf. Control*, **43** (2014), 257–263. https://doi.org/10.3724/SP.J.1219.2014.00257

31. Y. Xie, Y. Li, Z. Long, C. Dai, Discrete second-order nonlinear tracking-differentiator based on boundary characteristic curves and variable characteristic points and its application to velocity and position detection system, *Acta Autom. Sin.*, **40** (2014), 952–964. http://dx.doi.org/10.3724/SP.J.1004.2014.00952

32. H. Zhang, Y. Xie, G. Xiao, C. Zhai, Z. Long, A simple discrete-time tracking differentiator and its application to speed and position detection system for a maglev train, *IEEE Trans. Control Syst. Technol.*, **27** (2019), 1728–1734. https://doi.org/10.1109/TCST.2018.2832139

33. M. Athans, P. L. Falb, *Optimal Control: An Introduction to the Theory and Its Applications*, Courier Corporation, 2007.

34. D. E. Kirk, *Optimal Control Theory: An Introduction*, Courier Corporation, 2004.

35. J. Sun, K. Hang, Analysis and synthesis of time-optimal control systems, *IFAC Proc. Volumes*, **1** (1963), 347–351. https://doi.org/10.1016/S1474-6670(17)69673-3

36. X. Wang, Rapid-convergent nonlinear differentiator, *Mech. Syst. Signal Process.*, **28** (2012), 414–431. https://doi.org/10.1016/j.ymssp.2011.09.026

37. W. Chen, J. Yang, L. Guo, S. Li, Disturbance-observer-based control and related methods—an overview, *IEEE Trans. Ind. Electron.*, **63** (2015), 1083–1095. https://doi.org/10.1109/TIE.2015.2478397

AIMS Press